



Article

Multi-Sensor, Active Fire-Supervised, One-Class Burned Area Mapping in the Brazilian Savanna

Allan A. Pereira ^{1,*}, Renata Libonati ^{2,3,4} , Julia A. Rodrigues ² , Joana Nogueira ⁵ , Filippe L. M. Santos ^{2,6} , Duarte Oom ^{4,7} , Waislan Sanches ^{1,2}, Swanni T. Alvarado ^{8,9} and José M. C. Pereira ⁴

- ¹ Instituto Federal de Educação, Ciência e Tecnologia do Sul de Minas Gerais, Muzambinho 37890-000, MG, Brazil; waislanluis@gmail.com
- ² Departamento de Meteorologia, Instituto de Geociências, Universidade Federal do Rio de Janeiro, Rio de Janeiro 21941-916, RJ, Brazil; renata.libonati@igeo.ufrj.br (R.L.); juliarodrigues@igeo.ufrj.br (J.A.R.); flms.dcl20@uea.edu.br (F.L.M.S.)
- ³ Instituto Dom Luiz, Faculdade de Ciências, Universidade de Lisboa, 1749-016 Lisboa, Portugal
- ⁴ Forest Research Centre, School of Agriculture, University of Lisbon, 1349-017 Lisboa, Portugal; duarte.oom@ec.europa.eu (D.O.); jmcperreira@isa.ulisboa.pt (J.M.C.P.)
- ⁵ Institut für Landschaftsökologie, Westfälische Wilhelms (WWU)—Universität Münster, 48149 Münster, Germany; joana.nogueira@uni-muenster.de
- ⁶ Programa de Pós-Graduação em Clima e Ambiente (CLIAMB), Instituto Nacional de Pesquisas da Amazônia (INPA) e Universidade do Estado do Amazonas (UEA), Manaus 69060-001, AM, Brazil
- ⁷ European Commission, Joint Research Centre, 21027 Ispra, Italy
- ⁸ Programa de Pós-graduação em Agricultura e Ambiente, Centro de Estudos Superiores de Balsas, Universidade Estadual de Maranhão (UEMA), Balsas 65800-000, MA, Brazil; swanniromero@professor.uema.br
- ⁹ Programa de Pós-graduação em Geografia, Natureza e Dinâmica do Espaço, Universidade Estadual do Maranhão (UEMA), São Luís 65055-970, MA, Brazil
- * Correspondence: allan.pereira@ifsuldeminas.edu.br; Tel.: +55-35-991885985



Citation: Pereira, A.A.; Libonati, R.; Rodrigues, J.A.; Nogueira, J.; Santos, F.L.M.; Oom, D.; Sanches, W.; Alvarado, S.T.; Pereira, J.M.C. Multi-Sensor, Active Fire-Supervised, One-Class Burned Area Mapping in the Brazilian Savanna. *Remote Sens.* **2021**, *13*, 4005. <https://doi.org/10.3390/rs13194005>

Academic Editor: Ioannis Gitas

Received: 30 June 2021

Accepted: 28 September 2021

Published: 6 October 2021

Publisher's Note: MDPI stays neutral with regard to jurisdictional claims in published maps and institutional affiliations.



Copyright: © 2021 by the authors. Licensee MDPI, Basel, Switzerland. This article is an open access article distributed under the terms and conditions of the Creative Commons Attribution (CC BY) license (<https://creativecommons.org/licenses/by/4.0/>).

Abstract: Increasing efforts are being devoted to understanding fire patterns and changes highlighting the need for a consistent database about the location and extension of burned areas (BA). Satellite-derived BA mapping accuracy in the Brazilian savannas is limited by the underestimation of burn scars from small, fragmented fires and high cloudiness. Moreover, systematic mapping of BA is challenged by the need for human intervention in training sample acquisition, which precludes the development of automatic-generated products over large areas and long periods. Here, we developed a multi-sensor, active fire-supervised, one-class BA mapping algorithm to address several of these limitations. Our main objective is to generate a long-term, detailed BA atlas suitable to improve fire regime characterization and validation of coarse resolution products. We use composite images derived from the Landsat satellite to generate end-of-season maps of fire-affected areas for the entire Cerrado. Validation exercises and intercomparison with BA maps from a semi-automatic algorithm and visual photo interpretation were conducted for the year 2015. Our results improve the BA mapping by reducing omission errors, especially where there is high cloud frequency, few active fires are detected, and burned areas are small and fragmented. Finally, our approach represents at least a 45% increase in BA mapped in the Cerrado, in comparison to the annual extent detected by the current coarse global product from MODIS satellite (MCD64), and thus, it is capable of supporting improved regional emissions estimates.

Keywords: Landsat; VIIRS; machine learning; one-class classification; Cerrado; burned area

1. Introduction

The high global variability of fire occurrence makes it difficult to have a consistent fire record over space and time. Several studies indicate that fire acts as a determining factor for the ecology of the Brazilian savannas (Cerrado) [1,2]. However, in recent years, wildfires have been more frequent, modifying the fire regime of this biome as a result of

anthropic action [3]. Fire records are essential to understand trends and patterns of fire regimes. However, this is challenging for a continental biome like the Cerrado, with large extent, low accessibility areas, and inconsistent or scarce field fire records. In this context, remote sensing data, together with automatic classification techniques, are the only feasible, cost-effective, and timely source of information for systematic monitoring of fire occurrence for a broad range of spatial scales [4–6]. Earth observation satellite data allow analysis of large and remote areas affected by fire that are otherwise unevenly sampled by in situ field campaigns. Moreover, satellite information enables the generation of continuous, homogeneous, and long-term burned area (BA) databases. Over the last decades, the region has benefited from several approaches at different scales (global, regional, and local) that jointly address the complexity of automatically retrieving BA information from satellite imagery. Burnt area maps over the Cerrado have been mostly produced using spatially coarse data from the Moderate-Resolution Imaging Spectroradiometer (MODIS) sensor on board TERRA and AQUA satellites. Those maps have been systematically available since 2001 at global (e.g., MCD64-500 m [7], Fire CCI-250 m [8]) and regional (e.g., AQM-1 km [5]) scales. Although not operationally, other automatic BA classifiers were successfully applied to the region with diverse broad spatial coverage using other sensors, such as the Project for On-Board Autonomy-Vegetation (PROBA-V) [6] and the Visible Infrared Imaging Radiometer Suite (VIIRS) [9,10]. Validation and intercomparison exercises over the region reveal that estimates of BA using those coarse products present similar inter-annual variability but differ markedly in terms of total extent [5]. The regions with high frequency of medium and small fire scars present a challenge to those broad spatial resolution BA products [5–11]. Such limitations are a major drawback for regional applications, including fire and environmental management and formulation of public policies [12–15].

Several studies have pointed out the need for higher spatial resolution and longer-term BA records, to provide detailed information about small and fragmented burns and to advance the study of past, present, and future BA changes in tropical savannas [16–19]. In addition, this kind of information may be useful for benchmarking and validating coarse-resolution BA global/continental products in an effective and low-cost manner, by comparison with in situ measurements and airborne surveys [4,20–23]. A long-term dataset offers the opportunity to evaluate the temporal stability of the BA products, which refers to accuracy variability over time [21]. The series of Landsat satellites provides the longest temporal record of space-based observations across large areas, with higher spatial detail (30 m) and spectral resolution. These satellites offer a unique record of data for fire regime characterization and its change over time, dating back to the early 1970s [23]. The relatively high spatial resolution of Landsat-derived BA products is counterbalanced by the 16-day frequency of satellite overpasses. This limited frequency of image acquisition is often coupled with the presence of cloud cover and smoke aerosols, hampering the observation of burned areas. The ephemeral character of the radiative signal is a major limitation for burned area monitoring in tropical savannas [4,5,19,24–26]. In contrast with temperate and boreal regions, where it is possible to wait until the end of the fire season to map scars from previous months, in tropical savannas, the combustion residues are easily scattered by the wind, and the charcoal spectral signal quickly fades out [27]. Thus, the combined effect of cloudiness and the revisiting cycle of Landsat sensors contributes to omission errors in Landsat-derived BA products [25]. In addition, the varying number of cloud-free images available from different years complicates interannual BA comparison.

Pixel-based multi-temporal compositing methods are an alternative way to mitigate these limitations and have been widely used for BA detection with coarser resolution sensors [5,28–31], since they also contribute to reducing residual atmospheric effects [28]. Since the beginning of the open access Landsat era, in 2008, several studies have exploited compositing approaches to map the spatial-temporal patterns of environmental variables, such as deforestation and other land cover changes [32,33]. More specifically, burned area algorithms making use of temporal composites from the Landsat archive are also emerging worldwide. For example, [28] proposed an operative tool to obtain U.S. burned

area maps from Landsat data, using temporal compositing [16,34] and combining weekly Landsat composite imagery with MODIS active fires, to systematically map burned areas at 30m resolution. Similarly, [35] applied a composite of Landsat Thematic Mapper (TM) time series for classifying burnt areas in Australia from 1986 to 2013. A recent study [36] has used annual composites to produce maps of burned areas over the entire U.S. for the full-temporal Landsat archive. Other authors [37] developed an annual BA product using a random forest algorithm and [38] presented a machine learning approach to map burned areas over Asia, using composites of differential spectral-indices and three different classifiers, Classification and Regression Tree, Random Forest, and Support Vector Machine (SVM), both in the Google Earth Engine (GEE) platform [39]. Although a variety of studies applying Landsat image composites for burned area mapping have been successfully conducted worldwide, to date, there are few initiatives over the Cerrado region [40,41].

Another notable limitation of most BA mapping algorithms is the need for human intervention in training sample acquisition [28,40–43], making it a challenge to maintain operational products over large areas and long periods. This limitation may be circumvented by exploring two specific aspects of the problem: the relationship between active fires and burned areas and the possibility of envisaging BA mapping under the framework of one-class classification [44]. Since the observation of an active fire produced by vegetation burning typically is associated with the subsequent appearance of a burned area at the same location, active fires may be used to automatically select training samples for burned area mapping. By framing BA mapping as a one-class classification problem, no other training samples will be needed. This approach was implemented by [6,11], using the support vector data description and maximum entropy algorithms, respectively. Other BA mapping studies have relied on active fires as seeds for seeded region-growing in two-step classification approaches [45]. A drawback of this procedure is that burned area patches missing an active fire seed, e.g., due to short duration of the fire, or cloudiness at the time of overpass, will be omitted in the classification. This problem is avoided in the active fire-trained, one-class classification approach, which uses active fires not as spatial seeds but as spectral samplers for burned areas [6,11]. The approach we propose in this work is characterized by (i) the use of detection of changes based on temporal composites and (ii) an automated procedure to produce longer time series of fire scars in large areas without human intervention, namely, (a) the integration of active fire data to collect training samples and (b) use of a single class classification based on machine learning.

The methodology is based on our previous works [6,10], in which automated BA algorithms tailored for the PROBA-V and VIIRS sensors were developed and successfully applied to the Cerrado. The algorithm proposed here is based on samples collected from VIIRS active fire and the One-Class Support Vector Machine classifier applied to Landsat 8 OLI (Operational Land Imager) composite images. The results were evaluated over an area of 13,680,000 ha and compared against two available BA datasets, both considering change detection between consecutive Landsat images, one based on a semi-automatic algorithm [41] and the other derived from in situ analysis and visual photo interpretation [46,47]. Finally, the approach is applicable to generate fine-scale atlas of end-of-season fire scars for the entire Brazilian savanna in GEE.

2. Materials and Methods

2.1. Study Area

The study area covers four Landsat scenes (path/row: 218/072, 218/073, 219/070, and 219/071) located in southeastern Brazil and encompassing 13,680,000 ha (Figure 1). This area comprises conservation units mosaic from Upper Middle São Francisco River basin and from Serra do Espinhaço, considered of high ecological relevance due to high vegetation diversity and degree of ecological conservation [48]. The region is characterized by large extensions of rupestrian fields that challenge satellite-derived burned area classification due to the large amount of exposed rocks and sandstone soils, which can generate spectral confusion with burned areas [49]. Another challenge related to BA classification in

rupestrian fields is the ephemeral character of the spectral signals of burned areas [50]. The predominant biome in the study area is the Cerrado, with transition zones from Atlantic Forest and Caatinga biomes [51]. In the Upper Middle São Francisco region (219/070 and 219/071 scenes), the topography is marked by plateaus and depressions characterized as flat or moderately undulated relief [51,52]. The Serra do Espinhaço region (218/072 and 218/073 scenes) has a greater variety of reliefs, with strongly undulated, mountainous or steep, undulated and flat, and moderately undulated regions. This region contains a 1200 km long mountain range (i.e., Serra do Cipó National Park—NP), extending from the south-central region of Minas Gerais state to Chapada Diamantina, in the state of Bahia [53]. The highest point of this mountain range is at an altitude of 2044 m, located in Landsat scene 218/073.

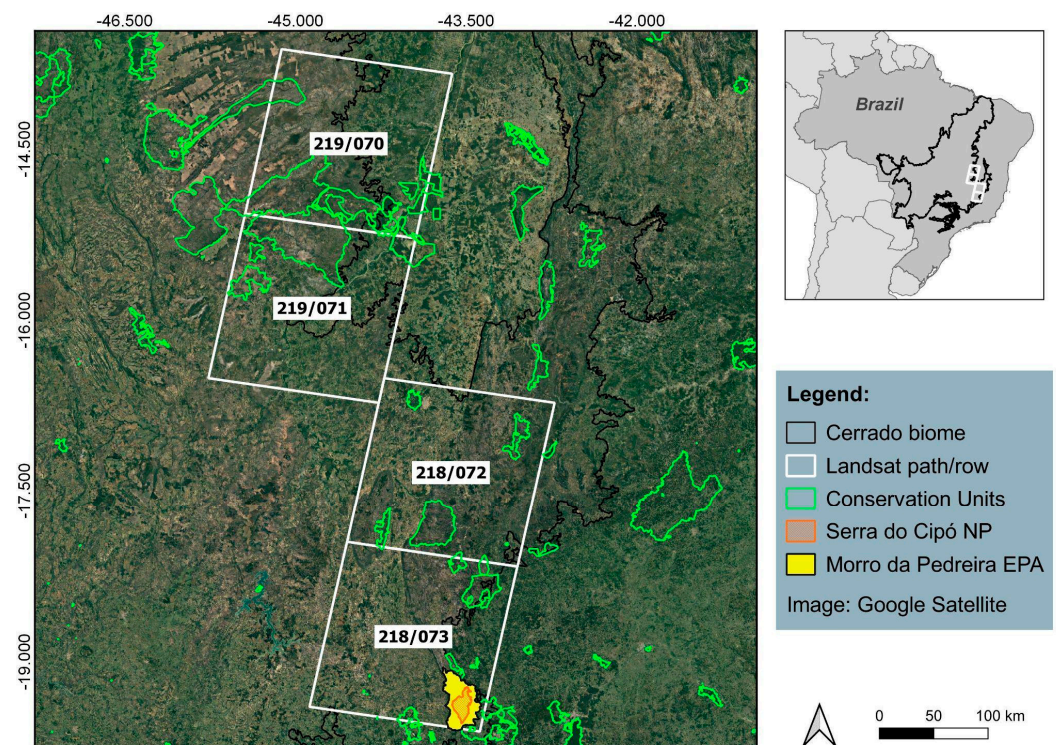


Figure 1. Spatial distribution of the Brazilian Cerrado (black outline in the small image) showing the four Landsat paths/rows (white squares) used in this study, highlighting the two conservation units (Serra do Cipó NP in orange and Morro da Pedreira EPA in yellow) selected as study areas for local evaluation of the algorithm performance. Green polygons indicate the location of the remaining conservation areas.

The Morro da Pedreira is an Environmental Protection Area (EPA) also contained in scene 218/073. This region is characterized by the transition from the Atlantic Forest to the Cerrado biomes, with the presence of different plant physiognomies linked to each biome type. The Morro da Pedreira EPA was chosen for comparison of the burned area products (described below), due to the availability of visually mapped burn data and to the ecological importance of the area [46,47].

The site at Serra do Espinhaço mountain range was selected because its abundant rock outcrops and terrain shading are prone to spectral confusion with burned areas, and we considered it important to test the algorithm performance under such challenging conditions. The other sites are located in areas Cerrado “sensu stricto”, the predominant vegetation type of the Cerrado biome, and were primarily chosen for their representativeness.

2.2. Datasets

2.2.1. Algorithm Development Dataset

The burned area algorithm was based on images from the OLI sensor of Landsat 8 satellite Collection 1–Level 1, downloaded from the United States Geological Survey database [54]. We used data from the near infrared (NIR–band 5 with 0.8 μm), short wave infrared (SWIR1–band 6 and SWIR2–band 7 with 1.6 and 2.1 μm , respectively), and the Landsat Quality Band Assessment (QA) band, which contains the cloud and water masks. The images were evaluated from July to December 2015, based on availability and total cloud cover. The 24 images evaluated are described in Table 1 for each Landsat scene. It is important to highlight that we aim to develop burned area maps at the end of fire season. Thus, the dates of the images used cover more than 90% of fire occurrences in the Cerrado [5].

Table 1. Landsat scenes (path/row) and dates of the OLI images used in this study. T1 indicates the pre-fire image obtained for each Landsat scene.

Landsat Scenes	Dates
218/072–218/073	30 July 2015 (T1)
	15 August 2015
	31 August 2015
	16 September 2015
	02 October 2015
	03 November 2015
219/070–219/071	06 August 2015 (T1)
	07 September 2015
	23 September 2015
	09 October 2015
	10 November 2015
	12 December 2015

We used the daily active fires (AF) dataset derived from the VIIRS sensor on board the Suomi-National Polar-orbiting Partnership satellite [55] at 375 m of spatial resolution, to capture small, namely sub-pixel, areas of flaming combustion. These data were obtained from the Brazilian Institute of Spatial Research (INPE) active fires database [56]. Due to its higher spatial resolution, the VIIRS active fire product has the ability to detect smaller events than the corresponding MODIS product and has been preferred for use in hybrid algorithms [55]. The revisit time from VIIRS is twice a day.

2.2.2. Intercomparison Datasets

An intercomparison of our results was undertaken against two Landsat-8/OLI-derived burned area available databases, one based on a semi-automatic algorithm (AQM30m) and the other one derived from in situ analysis and visual photo interpretation (AQMView). The AQM30m is a semi-automatic, unsupervised system to identify burned areas over the entire Cerrado, using pairs of close-date images from the Thematic Mapper (TM) and OLI sensors. It combines the analysis of temporal changes in Normalized Difference Vegetation Index (NDVI) and Normalized Burn Ratio Long SWIR Variation (NBR2) [41]. The product was downloaded from [57] for the same location and period described in Table 1. The AQMView [46,47] is a manually derived burned area map based on in situ verification and visual photointerpretation of Landsat Enhanced Thematic Mapper Plus (ETM+), TM, and OLI images by using RGB composites from 5 (1.6 μm), 4 (0.8 μm), and 3 (0.6 μm) bands for ETM+ and TM and 6 (1.6 μm), 5 (0.8 μm), and 4 (0.6 μm) for OLI. The dataset encompasses the period of 1984 to 2015 [46,47] over Morro da Pedreira EPA and Serra do Cipó NP (Landsat path/row 218/073) (Figure 1).

2.3. Methods

2.3.1. Algorithm Theoretical Basis

The proposed algorithm, hereafter the Landsat Burned Area Algorithm (AQM-LS), is a multi-sensor approach, which combines time series of surface reflectance from OLI sensor with temporal and spatial information derived from VIIRS AF data. Here we use an adaptation of our two previous works, the AQM-PROBA [6] and the AQM-VIIRS algorithms [10]. Both AQM-PROBA and AQM-VIIRS use the One-Class Support Vector Machine (OC-SVM) classifier and automated sample selection based on active fires.

The OC-SVM technique is derived from the standard Support Vector Machine algorithm [58,59] and designed to solve single-class classification problems, showing positive results in BA mapping when compared to other traditional methods [6,47,60–62]. The advantage of single class classifiers is that they do not require training samples from unburned areas, typically characterized by a wide variety of spectral signals [6].

Following our two previous works [6,10] the main stages of the algorithm are (i) multi-temporal compositing in the period when active focuses are concentrated, (ii) screening of samples collected at active hotspots, and (iii) choice of the kernel and classifier parameter tuning. The multi-temporal compositing criterion was minimization of Normalized Burned Ratio 2 (NBR2, Equation (1)) [61] meaning that the date with the lowest value of NBR2 was selected at each pixel in the composite image. Screening of the samples automatically collected at the locations of active fires is done using thresholds defined by data distribution, with natural breaks segmentation [6]. This step is necessary due to the differences in spatial resolutions between AF and Landsat images, which can lead to selection of training samples associated with AF located outside the burn scars. The choice of kernel and parameter ν and γ tuning is done by cross validation, as in [26]. These parameters indicate a greater or lesser permissiveness in mapping the burned area. Finally, tuning of the classification model is based on the results from the previous stage.

$$\text{NBR2} = (\text{SWIR2} - \text{SWIR1}) / (\text{SWIR2} + \text{SWIR1}) \quad (1)$$

where

SWIR1—band 6 and SWIR2—band 7 with 1.6 and 2.1 μm , respectively.

The main characteristics of the three algorithms are depicted in Table 2. Besides the spatial and temporal resolution, the main adaptations to the original algorithms are related to both spectral index and compositing techniques used. Here, we use the Landsat SWIR1 and SWIR2 bands to calculate the NBR2. The choice of this index is based on the work of [49], which shows greater separability between the classes of burned and unburned areas in Cerrado regions. Then, we create multi-monthly composites with the minimum NBR2 criterion [63,64] to build post-fire (T2) composites and to calculate the difference between T2 composite and the pre-fire image (T1) (first image available before the T2 composite), $\Delta\text{NBR2} = \text{NBR2}_{\text{T2}} - \text{NBR2}_{\text{T1}}$. The ΔNBR2 is bounded from -2 to $+2$, and typically values $\Delta\text{NBR2} < 0$ indicate burning. The ΔNBR2 has been used in several studies as an index to detect burned areas [41,49,65]. The corresponding date of the minimum NBR2 value for post fire composites is also retained, as an approximate date of burning.

To generate the training dataset required for the training samples in the AQM-LS algorithm, five steps were taken: (i) identification of the NBR2T2 and ΔNBR2 composites that overlapped the AF VIIRS pixels in space and time, (ii) selection of the AF pixels with dates preceding the date of the pixel selected for the minimum NBR2 composite, (iii) extraction of NBR2T2 and ΔNBR2 pixel values based on the AF identified in i and ii followed by (iv) a segmentation procedure using the Jenks natural breaks algorithm [63] which divides data distribution into three classes. Thus, only active fires located in the class with the lower NBR2 values and the highest difference value between NBR2 T1 and T2 are chosen to train the classifier. The OC-SVM parameters used were based on [6] with $\gamma = 0.1$ and $\nu = 0.005$. The γ parameter is the inverse of the radius of influence of samples selected by the model as support vectors, i.e., it controls how far the influence of a single training example reaches. ν defines the trade-off between model overfitting

and generalization, and thus controls the number of support vectors used. (v) Finally, the classifier returns positive values for classes that are similar to those in the training sample and negative values otherwise, classifying burned, unburned, and unmapped areas as recommended by [66]. Thus, the final end-of-season map consists of the three classes (burned, unburned, and unmapped) and includes the date of each fire scar, obtained from the layer of the Landsat image dates selected for each pixel in the composite image. Moreover, AQM-LS provides two additional layers containing the number of images used and the cloud cover recurrence in each pixel. That information may be used as quality-flags to identify high and low confidence in the burned and unburned classes.

Table 2. Comparison between previous BA algorithms: AQM-PROBA, AQM-VIIRS, and the algorithm developed in this work, AQM-LS.

	AQM-PROBA	AQM-VIIRS	AQM-LS
Reference	[5]	[9]	this work
Spatial Resolution (m)	300	375	30
Temporal Resolution (days)	5	1	16
Channels	NIR (0.84 μm)	NIR (0.86 μm) MIR (3.74 μm) TIR (11.45 μm)	SWIR1 (1.6 μm) SWIR2 (2.1 μm)
Satellite Temporal coverage	2013–2018	2012–present	1985 *–present
AF data	VIIRS 375 m	VIIRS 375 m	VIIRS 375 m
Spectral index	none	(V,W) [62]	NBR2 [63]
Compositing technique	second minimum NIR	minimum W	minimum NBR2

* Based on Landsat availability over the region.

2.3.2. Intercomparison and Validation Approaches

Any attempt to validate retrieved burned scars from Landsat 30 m imagery is challenged by the virtual absence of in situ measurements and higher resolution remote sensing data. This limitation was circumvented here by creating a reference dataset based on information derived from visual photo interpretation [67]. This reference dataset was based on selection of 20,000 points with random spatial distribution [68] over the multi-temporal composites of Landsat RGB 567 bands and NBR2 for burned and unburned classes. A total of 5000 pixels were randomly distributed over each Landsat scene. AFs were also used to improve the selection of burned pixels. A total of 811 pixels were classified as burned and 19,189 pixels in the remaining land cover types (namely, green vegetation, crop fields, and water bodies) as the unburned class (4.1% burned and 95.9% unburned pixels) (Table 3).

Table 3. Number of randomly distributed points for each Landsat scene in the burned and unburned classes.

Path/Row	Validation Sample Points			
	Burned		Unburned	
	Points	%	Points	%
218/073	187	3.7	4813	96.3
218/072	152	3.0	4848	97.0
219/070	327	6.5	4673	93.5
219/071	145	2.9	4855	97.1
Total	811	4.1	19,189	95.9

Validation was performed through a cross tabulation between the reference dataset and the burned area maps from AQM-LS and AQM30m, using scalar attributes derived from the 2×2 contingency table [69] (Table 4). Four validation metrics were used to verify

the validation approach, namely, omission error (OE), commission error (CE), bias (BIAS), and the critical success index (CSI) (Table 5). The OE indicates the discrimination power of the classifier through the fraction of observed burned pixels that turn out to be classified as unburned. The CE reflects the reliability of the classifier through the fraction of classified burned pixels that turn out to be incorrect. Both OE and CE have a negative orientation. BIAS greater (less) than one indicates that burned pixels were classified more (less) often than observed. Unbiased classification exhibits BIAS equal to 1. The CSI is a measurement of accuracy reflecting the correspondence between the classification and the reference, considering only the class of interest, i.e., burned area. The CSI varies between 0 (worst) and 1 (best).

Table 4. Generic contingency table between the reference and burned area (BA) products.

		Reference	
		Burned	Unburned
BA Products	Burned	A	B
	Unburned	C	D

Table 5. Validation metrics, acronyms, and equations derived from the contingency table described in Table 4.

Validation Metrics	Acronym	Equation
Omission Error	OE	$C/(A + C)$
Commission Error	CE	$B/(A + B)$
Bias	BIAS	$(A + B)/(A + C)$
Critical Success Index	CSI	$A/(A + B + C)$

A quantitative intercomparison of the results from AQM-LS was also undertaken by using two Landsat-8/OLI-derived burned area databases, one based on a semi-automatic algorithm (AQM30m) and the other one derived from in situ analysis and visual photo interpretation (AQMView). The intercomparison with the latter was conducted over the Morro da Pedreira EPA and with the former was carried out over the 5000 points randomly distributed over each Landsat scene (Table 3).

Finally, we evaluated the capacity of the AQM-LS algorithm to classify burned areas associated with active fires omissions. To that end, we evaluated the number of fire scars containing active fires. The analysis was performed for four classes of scars sizes, namely, (i) 0–25 ha, (ii) 25–100 ha, (iii) 100–1000 ha, and (iv) > 1000 ha. The choice of these classifications was based on the work by [6] who performed a similar analysis for the Cerrado region.

3. Results

3.1. Classification of Burned Area Scars and Accuracy Assessment

We first evaluated the total extent of BA retrieved by the AQM-LS and compared the results with those from the AQM30m product for the same period (Table 1). Figure 2 shows the comparison of both products for the four Landsat scenes. The BA retrieved by AQM-LS and AQM30m was in general similar in location (Figure 2a), albeit very divergent in magnitude. The AQM-LS algorithm identified a total of 447,700 ha of burned area, corresponding, to 7.5%, 3.9%, 3.1%, and 2.8% of Landsat scene 219/070, 218/073, 218/072, and 219/071, respectively (Figure 2b). By contrast, the AQM30m detected 30% less BA, representing 311,000 ha for the same period. The greatest difference between the AQM-LS and the AQM30m was found in scene 218/073, where the latter product estimated only half as much burned area. In scenes 218/072, 219/071, and 219/070, these differences are 41%, 34%, and 12%, respectively.

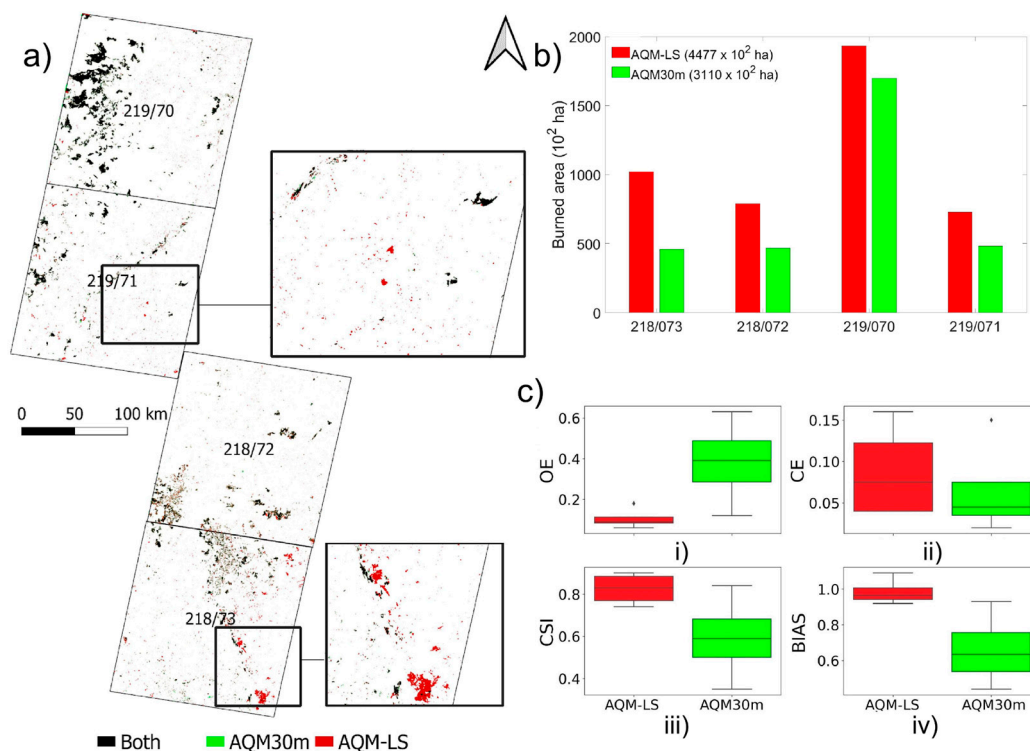


Figure 2. (a) Fire scars as detected by AQM-LS (red), AQM30m (green) and by both products (black) for the period and regions depicted in Table 1. Gray polygon shows the four Landsat scenes boundary. (b) Total amount of burned area ($\times 10^2$ ha) as detected by BA products for each Landsat scene. Numbers in parentheses denote the total amount of burned area for all Landsat scenes. (c) Validation metrics: (i) Omission errors (OE), (ii) Commission errors (CE), (iii) Critical Success Index (CSI), and (iv) Bias (BIAS) for AQM-LS (red) and AQM30m (green) products in all Landsat scenes.

The statistical analysis of the accuracy assessment for both AQM-LS and AQM30m products on a pixel basis, derived from the contingency table and considering each of the four Landsat scenes is presented in Figure 2c. Overall, the AQM-LS product displays higher CSI values for all the Landsat scenes, in comparison with the AQM30m product. The AQM-LS product has much lower OE than AQM30m, while both products show very low CE. The underestimation by AQM30m is reflected in values of BIAS much lower than one. An example of the contrast between OE of the two BA algorithms is provided in Figure 3, which shows a fire scar with more than 8000 ha in Serra do Cipó NP. This fire event occurred between 16 and 20 October 2015 (Landsat scene 218/073) and was mapped by the AQM-LS product (in red) and confirmed by the presence of VIIRS active fires but omitted by the AQM30m product (in green). Indeed, the larger discrepancies between the two products occurred also in the scene 218/073, which is frequently cloudy (Figure 3); thus, the change detection based on temporal multitemporal composite approach adopted by AQM-LS performs much better than change detection approaches based on pairs of images used in the AQM30m product. In this region, cloud recurrence, defined as the number of times that a pixel is covered by clouds over the study area from 30 July to 3 November, reached the same pixels in every 5 dates. We observed high omission cases from AQM30m in cloudy areas, but by contrast, AQM-LS omitted few fire scars (Figure 3), highlighting the effectiveness of the compositing technique to minimize omission errors in cloudy areas.

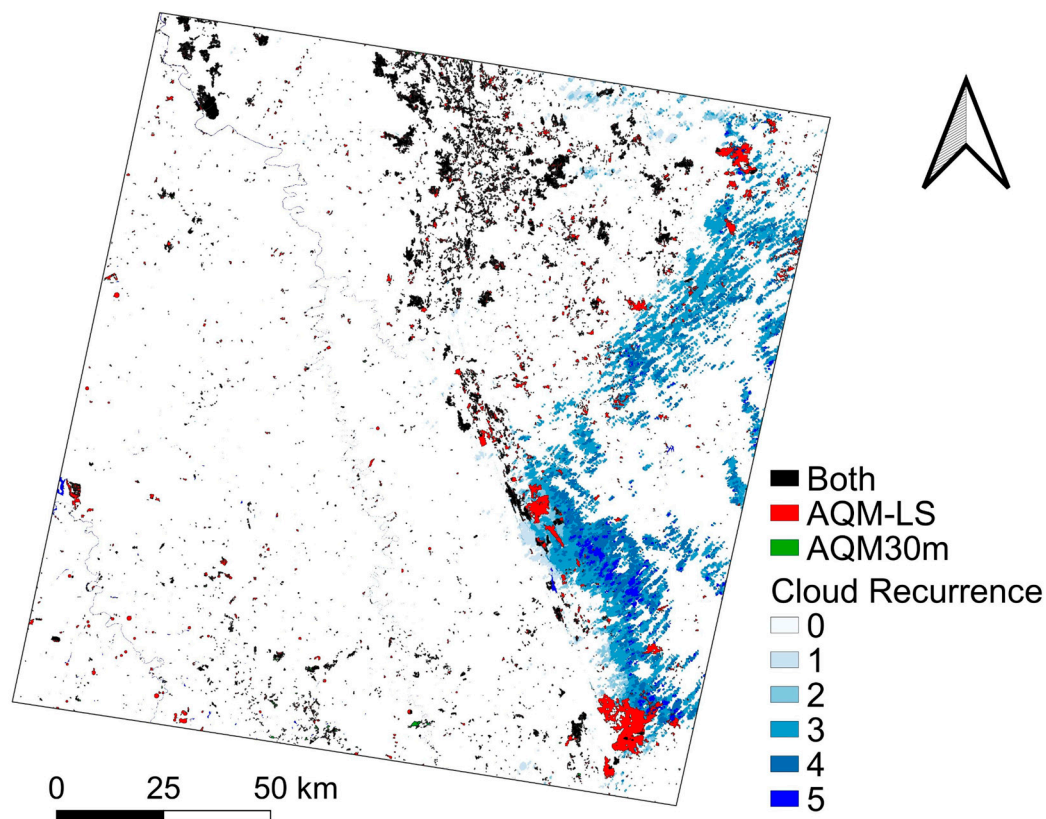


Figure 3. Fire scars as detected by AQM-LS (red) (1020 km²), AQM30m (green) (460 km²) and by both products (black) (413 km²) for Landsat scene 218/073, highlighting cloud recurrence (number of times that a pixel is covered by clouds over study areas, in blue, in # scenes in the post-fire composite) during the period depicted in Table 1.

3.2. Intercomparison among Automatic and Manual BA Algorithms

Here, we provide an intercomparison between the automatic (AQM-LS and AQM30m) and manually derived (AQMView) burned area maps at Morro da Pedreira EPA. In this case, the AQM-LS classified a similar extent of burned area as AQMView, 13,670 and 15,346 ha, respectively (Figure 4). This corresponds to approximately six times more burned area than that mapped by AQM30m (2236 ha). This difference is observed especially in the detection of small fires, which are omitted by AQM30m in the northeastern and eastern parts of the study region (Figure 4a).

Around 85% of the BA detected by AQM-LS is coincident with the AQMView mapping, while the remaining 15% are distributed along the boundary of the fire scars, mainly in the extreme south and north of the region. By analyzing fire scars as a function of size, we observed that AQM-LS, AQM30m, and AQMView all have the highest frequencies of scars in the smallest size class (0–25 ha) (Figure 4b). For this and the second (25–100 ha) classes, AQM-LS detected more scars than AQM30m and AQMView. In the case of big fires (>100 ha), AQM-LS presents similar values as observed for AQM30m and AQMView. The AQM30m does not detect any scar in the larger class, reflecting the underestimation of two large fire scars that occurred in the south of the conservation unit (Figure 4a). Finally, the total value of the largest scar size recorded from 15 August to 3 November 2015 by each product corresponds to 8181 ha (AQM-LS), 588 ha (AQM30m), and 9894 ha (AQMView).

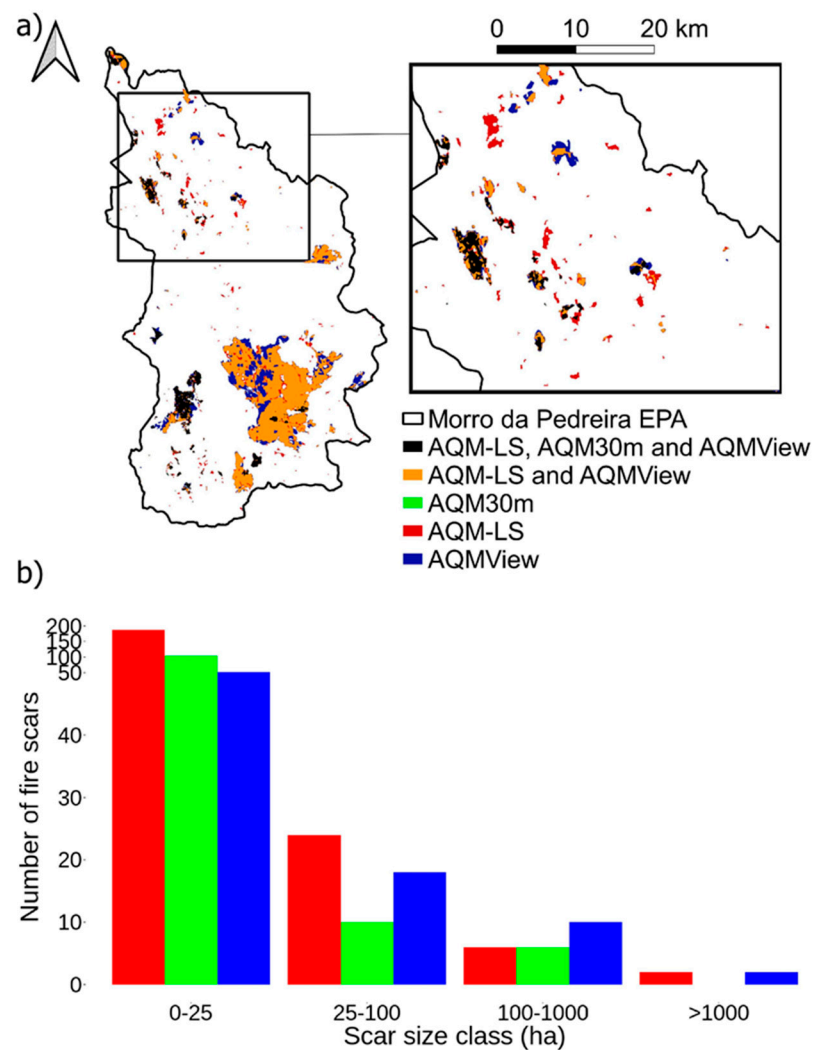


Figure 4. (a) Spatial distribution of burned area detected by AQM-LS (red), AQM30m (green), AQMView (blue), two products (namely AQM-LS and AQMView, orange), and the three products (black) in the Morro da Pedreira EPA (black outline) encompassing the Serra do Cipó NP from 15 August to 3 November 2015. (b) The corresponding total number of scars detected by BA products per scar size classes.

3.3. Towards a BA Atlas for the Entire Cerrado

To improve the process of classifying burnt areas, the algorithm was adapted for implementation on the digital cloud image processing platform GEE [39] for the entire Cerrado, from 2013 to 2020. This implementation is an important step towards the application of this method to systematically map burned areas in the entire Cerrado on an historical basis. To this end, our final burned area product provides three classes: burned, unburned, and unmapped pixels. Pixels that cannot be observed or interpreted either due to clouds or to sensor problems are classified as unmapped, to guarantee that only pixels with reliable data are included in the burned/unburned final map [70]. Moreover, auxiliary information is provided regarding the number of cloud-free pixels, cloud and water masks, and the date of BA detection. Figure 5 shows the comparison between AQM-LS and AQM30m for the 2015 year for the entire Cerrado. The total extent of BA detected by AQM-LS was 15,892,187 ha and 10,303,742 ha by AQM30m, meaning that AQM30 failed to detect 35% of the area detected by AQM-LS.

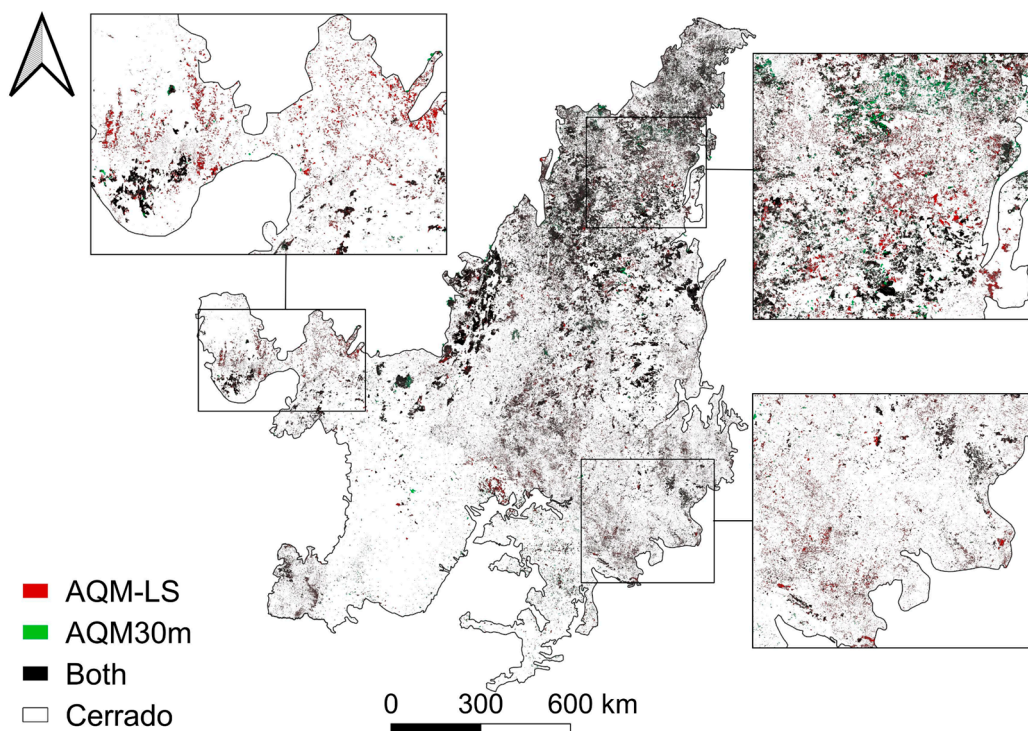


Figure 5. Spatial distribution of burned area detected by AQM-LS (red), AQM30m (green), and by both products (namely, AQM-LS and AQM30m, black) over Cerrado for 2015; insets show spatial detail of BA classification for areas in Northern, Southwestern, and Southeastern Cerrado.

4. Discussion

The focus of our approach was twofold: (i) to reduce the high omission levels from current algorithms, which rely on change detection approaches based on pairs of images and (ii) to allow the generation of long-term records suitable for trend analysis, using an approach with minimal human intervention. To this end, we used multi-sensor (Landsat and VIIRS), active fire-supervised, one-class burned area mapping. The methodology developed here performed very well at mapping burned areas at regional level, without the need for human supervision in the collection of burning samples. Reliable, automated, and historical record of burned areas at 30 m resolution and at the biome level has important applications for fire management [71], emission assessment [72], fire regime studies [73], and climate and land use/cover changes [74]. In addition to those applications, this kind of burned area product may serve as a basis for validation of burned area maps derived from satellite products with coarse spatial resolution.

AQM-LS was able to classify 54% and 45% more BA than the AQM30m and the annual amount provided by MCD64 [10], respectively. Thus, the smaller area detected by AQM30m in 2015 is very close to that obtained by MCD64 (10,954,230 ha), which is known for its underestimation of burned areas in Cerrado [10,75,76]. This low accuracy is generally attributed to MODIS coarse spatial resolution (500 m), which challenges the detection of small and highly fragmented fires, in particular, those associated with agricultural burns [11,40,76]. The comparison of Landsat medium- and MODIS coarse-resolution BA products at the continental scale of Cerrado not only confirms the very conservative behavior of MCD64 but also the strong underestimation of savanna fire emissions, as highlighted by previous studies in Africa [77].

The case study in the Morro da Pedreira EPA shows that AQM-LS detections follow a pattern close to the ‘reference’ map from AQMView, whereas AQM30m shows a less realistic burned area mapping (six times less than the former). This huge difference can have a substantial impact on the fire regime characterization, emissions estimates, and

validation of coarse resolution products. A manual mapping technique such as that used in AQMView allows a supervised analysis, as in cases where the burning under cirrus clouds can be classified, which is a limitation of remote sensing. On the other hand, it is prone to missing details that may escape to the human eye. The visual detection and manual delineation of the fire scars in the AQMView dataset was performed by using a standardized mapping scale of 1:25,000 and a standardized brightness and contrast parameters for all scenes [46], which could affect the accuracy of the delineation. This was evident in the analysis by size classes, where the AQM-LS detected more smaller fires (<25 ha) than the AQM30m and AQMView (Figure 4b).

The need for active fires information as seed points for burned pixel classification on region growing techniques was circumvented by using the active fire-trained, one-class classification approach, which uses active fires not as spatial seeds but as spectral samplers for burned areas. Our results highlight active fires omission, due to short duration of the fire, or cloudiness at the time of overpass, which has impact on the final burned area classification [5,6,27,45,78]. In this sense, the use of AF as a training sample for a classifier would fill this gap, making it possible to map burned areas even with the absence of AF, as shown in Figure 6. For instance, in *veredas* areas (Figure 6), the vegetation is characterized by the predominance of the palm tree *Mauritia flexuosa* species and peat soils, which leads to the occurrence of underground fires not detected by satellites [79]. It is also possible to observe omissions from active fires in areas where burning occurred at a low intensity [49] and in areas with dense layers of smoke, which reduces the radiometric signal [26].

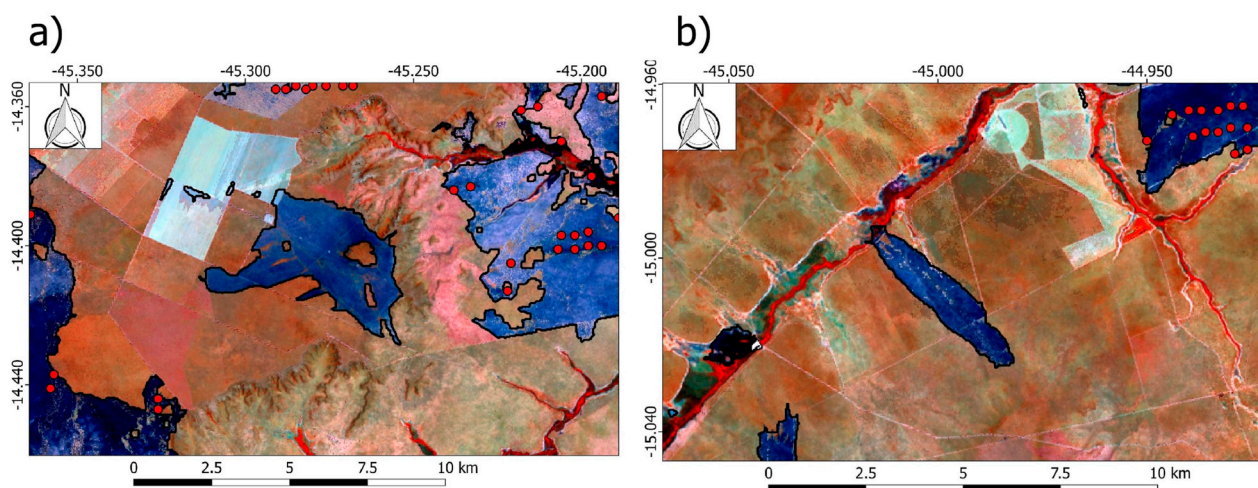


Figure 6. Burn scars (in blue) classified by AQM-LS algorithm in the presence of active fires (AF, respectively in red), highlighting two cases where burn scars were classified in the absence of AF: (a) burn scar with 852 ha and (b) burn scar with 368 ha. RGB 567 image composite from 6 August to 12 December 2015 for the 219/070 scene.

The differences between AQM-LS and AQM30m are observed in specific conditions, such as those that include the presence of high frequency clouds and also in rocky field areas. The results of the AQM-LS demonstrate greater accuracy, evidenced by smaller errors of omission when compared to the AQM30m. In this context, another relevant factor highlighted here is the use of change detection based on temporal composites to quantify the burned areas at the end of the fire season. The proposed algorithm provided competitive results and proved to be effective to produce more accurate results in the quantification of burned areas than the change detection based on pairs of images, proposed by AQM30m. This is because the composites merge the information of interest in a single image, minimizing the effects of clouds [30,31], as observed in scene 218/073, where the high concentration of clouds led to a high omission by the AQM30m and, in contrast, a low omission from the AQM-LS. The multitemporal compositing approach is frequently used in burned area mapping, especially using coarse spatial resolution data [16,34,49,65], but few

studies applied this technique to Landsat data, particularly in Cerrado. Thus, our results provide evidence for the suitability of Landsat multitemporal composites approaches to enhance BA detection in such a savannah-like ecosystem. Furthermore, AQM-LS shows improved capacity of BA classification in areas where there is spectral confusion between the burn signal and rocks.

Despite the promising results obtained, we acknowledge that there are limitations to the single class classifier, regarding the exclusion of pixels with high burning severity. This is because this classifier has the characteristic of excluding areas considered by the SVM as outliers. This limitation was also observed in previous works [6,10] and partially controlled with the application of mathematical morphology filters, considering the neighborhood of the areas classified as burned. Another limitation is the classifier parameters, which can be more permissive or more restrictive, resulting in errors of commission or omission. In this study, the choice of value parameters was made through cross-validation, which made it possible to adjust these parameters, according to the characteristics of the fires in each scene. For processing a large area, such as the entire Cerrado biome, the generalization of this index may cause errors in classification for regions with different fire regimes. In this context, for the generation of the end-of-season fire scar maps for the entire Brazilian savanna in GEE, we trained the model and fitted these parameters by partitioning the region into 19 subregions previously developed based on biophysical (rainfall patterns, topography, and land cover) [80] and fire [3] characteristics. It is worth mentioning that the selection of a single pre-fire (T1) image decreases the degree of automation of the BA mapping processing chain. In order to circumvent this issue, we made an adaptation in the implementation of AQM-LS in GEE concerning the pre-fire information. We considered the differences between successive composites instead of evaluating a single pre-fire (T1) image, i.e., we created multi-monthly composites with the minimum NBR2 criterion to build both post-fire (T2) and pre-fire (T1) composites and calculated the difference between T2 and T1 composites.

Machine learning is being used worldwide to improve burned area detection, particularly for Cerrado [6,9,10]. Here, we show that a machine learning approach based on multi-temporal composites and automated and regionalized sample selections, as a promising and flexible technique that can be applicable to regions with different fire patterns and characteristics, also contributes to minimizing the omission errors. It is worth noting that the algorithm presented here does not require human intervention and was developed using routines in GEE, making it possible to apply the method to other areas. Thus, future work is suggested to evaluate the application of the method in other biomes and areas with different fire regimes.

Author Contributions: A.A.P. and R.L. conceived and designed the experiments; A.A.P. and J.A.R. performed the experiments; A.A.P., R.L., J.A.R., F.L.M.S., J.N. and D.O. analyzed the data; J.M.C.P., W.S. and S.T.A. contributed to materials/analysis tools; A.A.P., R.L., J.N., J.M.C.P. and D.O. wrote the paper. All authors have read and agreed to the published version of the manuscript.

Funding: This work was developed under the scope of Project Andura [CNPq grant number 441971/2018–0]; J.N. was supported by the ‘Women in Research’-fellowship program, WWU Münster; J.A.R. was supported by CNPq [grant number 380779/2019–6]; F.L.M.S. was early supported by CNPq [grant number 381461/2018–1] and is financed by the Coordenação de Aperfeiçoamento de Pessoal de Nível Superior–Brasil (CAPES) - Finance Code 001 [grant number 88887.498119/ 2020–00]; R.L. was supported by CNPq [grant number 305159/2018–6] and FAPERJ [grant number E26/202.714/2019]; and FCT supports CEF [project UIDB/00239/2020] and IDL [project UIDB/50019/2020]. W.S. was supported by CNPq [grant number 180237/2020–9]. The authors would like to thank Alberto W. Setzer for contributions in the early stages of this work.

Institutional Review Board Statement: Not applicable.

Informed Consent Statement: Not applicable.

Data Availability Statement: The data presented in this study are available on request from the corresponding author.

Acknowledgments: The authors would like to thank Alberto W. Setzer for contributions in the early stages of this work.

Conflicts of Interest: The authors declare no conflict of interest.

References

- Coutinho, L.M. Aspectos Ecológicos do Fogo no Cerrado. II—As Queimadas e a Dispersão de Sementes em Algumas Espécies Anemocóricas do Estrato Herbáceo-Subarbustivo. *Bol. Botânica* **1977**, *5*, 57. [\[CrossRef\]](#)
- Pereira, A.C.; Oliveira, S.L.J.; Pereira, J.M.C.; Turkman, M.A.A. Modelling fire frequency in a Cerrado savanna protected area. *PLoS ONE* **2014**, *9*, 102380. [\[CrossRef\]](#)
- Silva, P.S.; Nogueira, J.; Rodrigues, J.A.; Santos, F.L.M.; Pereira, J.M.C.; DaCamara, C.C.; Daldegan, G.A.; Pereira, A.A.; Peres, L.F.; Schmidt, I.B.; et al. Putting fire on the map of Brazilian savanna ecoregions. *J. Environ. Manag.* **2021**, *296*, 113098. [\[CrossRef\]](#)
- Libonati, R.; DaCamara, C.C.; Pereira, J.M.C.; Peres, L.F. Retrieving middle-infrared reflectance for burned area mapping in tropical environments using MODIS. *Remote Sens. Environ.* **2010**, *114*, 831–843. [\[CrossRef\]](#)
- Libonati, R.; DaCamara, C.C.; Setzer, A.W.; Morelli, F.; Melchiori, A.E. An algorithm for burned area detection in the Brazilian Cerrado using 4 μm MODIS imagery. *Remote Sens.* **2015**, *7*, 15782–15803. [\[CrossRef\]](#)
- Pereira, A.; Pereira, J.; Libonati, R.; Oom, D.; Setzer, A.; Morelli, F.; Machado-Silva, F.; de Carvalho, L. Burned Area Mapping in the Brazilian Savanna Using a One-Class Support Vector Machine Trained by Active Fires. *Remote Sens.* **2017**, *9*, 1161. [\[CrossRef\]](#)
- Giglio, L.; Boschetti, L.; Roy, D.P.; Humber, M.L.; Justice, C.O. The Collection 6 MODIS burned area mapping algorithm and product. *Remote Sens. Environ.* **2018**, *217*, 72–85. [\[CrossRef\]](#)
- Lizundia-Loiola, J.; Otón, G.; Ramo, R.; Chuvieco, E. A spatio-temporal active-fire clustering approach for global burned area mapping at 250 m from MODIS data. *Remote Sens. Environ.* **2020**, *236*, 111493. [\[CrossRef\]](#)
- Pinto, M.M.; Libonati, R.; Trigo, R.M.; Trigo, I.F.; DaCamara, C.C. A deep learning approach for mapping and dating burned areas using temporal sequences of satellite images. *ISPRS J. Photogramm. Remote Sens.* **2020**, *160*, 260–274. [\[CrossRef\]](#)
- Santos, F.L.M.; Libonati, R.; Peres, L.F.; Pereira, A.A.; Narcizo, L.C.; Rodrigues, J.A.; Oom, D.; Pereira, J.M.C.; Schroeder, W.; Setzer, A.W. Assessing VIIRS capabilities to improve burned area mapping over the Brazilian Cerrado. *Int. J. Remote Sens.* **2020**, *41*, 8300–8327. [\[CrossRef\]](#)
- Campagnolo, M.L.; Oom, D.; Padilla, M.; Pereira, J.M.C. A patch-based algorithm for global and daily burned area mapping. *Remote Sens. Environ.* **2019**, *232*, 111288. [\[CrossRef\]](#)
- Flannigan, M.D.; Wotton, B.M. Climate, weather, and area burned. In *Forest Fires*; Elsevier: Amsterdam, The Netherlands, 2001; pp. 351–373.
- Le Quére, C.; Raupach, M.R.; Canadell, J.G.; Marland, G.; Bopp, L.; Ciais, P.; Conway, T.J.; Doney, S.C.; Feely, R.A.; Foster, P.; et al. Trends in the sources and sinks of carbon dioxide. *Nat. Geosci.* **2009**, *2*, 831–836. [\[CrossRef\]](#)
- Giglio, L.; Randerson, J.T.; van der Werf, G.R.; Kasibhatla, P.S.; Collatz, G.J.; Morton, D.C.; Defries, R.S. Assessing variability and long-term trends in burned area by merging multiple satellite fire products. *Biogeosciences* **2010**, *7*, 1171–1186. [\[CrossRef\]](#)
- Van der Werf, G.R.; Randerson, J.T.; Giglio, L.; Collatz, G.J.; Mu, M.; Kasibhatla, P.S.; Morton, D.C.; Defries, R.S.; Jin, Y.; van Leeuwen, T.T. Global fire emissions and the contribution of deforestation, savanna, forest, agricultural, and peat fires (1997–2009). *Atmos. Chem. Phys.* **2010**, *10*, 11707–11735. [\[CrossRef\]](#)
- Bastarrika, A.; Alvarado, M.; Artano, K.; Martinez, M.P.; Mesanza, A.; Torre, L.; Ramo, R.; Chuvieco, E. BAMS: A tool for supervised burned area mapping using landsat data. *Remote Sens.* **2014**, *6*, 12360–12380. [\[CrossRef\]](#)
- Pu, R.; Gong, P. Determination of burnt scars using logistic regression and neural network techniques from a single post-fire Landsat 7 ETM+ image. *Photogramm. Eng. Remote Sensing* **2004**, *70*, 841–850. [\[CrossRef\]](#)
- Kachmar, M.; Sánchez-Azofeifa, G.A. Detection of post-fire residuals using high- and medium-resolution satellite imagery. *For. Chron.* **2006**, *82*, 177–186. [\[CrossRef\]](#)
- Sa, A.C.L.; Pereira, J.M.C.; Vasconcelos, M.J.P.; Silva, J.M.N.; Ribeiro, N.; Awasse, A. Assessing the feasibility of sub-pixel burned area mapping in miombo woodlands of northern Mozambique using MODIS imagery. *Int. J. Remote Sens.* **2003**, *24*, 1783–1796. [\[CrossRef\]](#)
- Oliva, P.; Schroeder, W. Assessment of VIIRS 375 m active fire detection product for direct burned area mapping. *Remote Sens. Environ.* **2015**, *160*, 144–155. [\[CrossRef\]](#)
- Padilla, M.; Stehman, S.V.; Chuvieco, E. Validation of the 2008 MODIS-MCD45 global burned area product using stratified random sampling. *Remote Sens. Environ.* **2014**, *144*, 187–196. [\[CrossRef\]](#)
- Roy, D.P.; Boschetti, L.; Justice, C.O.; Ju, J. The collection 5 MODIS burned area product—Global evaluation by comparison Please confirm added location with the MODIS active fire product. *Remote Sens. Environ.* **2008**, *112*, 3690–3707. [\[CrossRef\]](#)
- Roy, D.P.; Wulder, M.A.; Loveland, T.R.; Woodcock, C.E.; Allen, R.G.; Anderson, M.C.; Helder, D.; Irons, J.R.; Johnson, D.M.; Kennedy, R.; et al. Landsat-8: Science and product vision for terrestrial global change research. *Remote Sens. Environ.* **2014**, *145*, 154–172. [\[CrossRef\]](#)
- Dacamara, C.C.; Libonati, R.; Barros, A.; Gaspar, G.; Calado, T.J. Using MODIS imagery to assign dates to maps of burn scars in Portugal. *Geophys. Res. Abstr. EGU Gen. Assem.* **2012**, *14*, 2012–12485.
- Hawbaker, T.J.; Radeloff, V.C.; Syphard, A.D.; Zhu, Z.; Stewart, S.I. Detection rates of the MODIS active fire product in the United States. *Remote Sens. Environ.* **2008**, *112*, 2656–2664. [\[CrossRef\]](#)

26. Schroeder, W.; Prins, E.; Giglio, L.; Csiszar, I.; Schmidt, C.; Morisette, J.; Morton, D. Validation of GOES and MODIS active fire detection products using ASTER and ETM+ data. *Remote Sens. Environ.* **2008**, *112*, 2711–2726. [[CrossRef](#)]
27. Pereira, J.M.C. Remote sensing of burned areas in tropical savannas. *Int. J. Wildland Fire* **2003**, *12*, 259–270. [[CrossRef](#)]
28. Boschetti, L.; Roy, D.P.; Justice, C.O.; Humber, M.L. MODIS-Landsat fusion for large area 30 m burned area mapping. *Remote Sens. Environ.* **2015**, *161*, 27–42. [[CrossRef](#)]
29. Barbosa, P.M.; Pereira, J.M.C.; Grégoire, J.M. Compositing criteria for burned area assessment using multitemporal low resolution satellite data. *Remote Sens. Environ.* **1998**, *65*, 38–49. [[CrossRef](#)]
30. Chuvieco, E.; Ventura, G.; Martín, M.P.; Gómez, I. Assessment of multitemporal compositing techniques of MODIS and AVHRR images for burned land mapping. *Remote Sens. Environ.* **2005**, *94*, 450–462. [[CrossRef](#)]
31. Stroppiana, D.; Pinnock, S.; Pereira, J.M.C.; Grégoire, J.M. Radiometric analysis of SPOT-VEGETATION images for burnt area detection in Northern Australia. *Remote Sens. Environ.* **2002**, *82*, 21–37. [[CrossRef](#)]
32. Hansen, M.C.; Egorov, A.; Potapov, P.V.; Stehman, S.V.; Tyukavina, A.; Turubanova, S.A.; Roy, D.P.; Goetz, S.J.; Loveland, T.R.; Ju, J.; et al. Monitoring conterminous United States (CONUS) land cover change with Web-Enabled Landsat Data (WELD). *Remote Sens. Environ.* **2014**, *140*, 466–484. [[CrossRef](#)]
33. Zhu, Z.; Woodcock, C.E. Continuous change detection and classification of land cover using all available Landsat data. *Remote Sens. Environ.* **2014**, *144*, 152–171. [[CrossRef](#)]
34. Hawbaker, T.J.; Vanderhoof, M.K.; Schmidt, G.L.; Beal, Y.J.; Picotte, J.J.; Takacs, J.D.; Falgout, J.T.; Dwyer, J.L. The Landsat Burned Area algorithm and products for the conterminous United States. *Remote Sens. Environ.* **2020**, *244*, 111801. [[CrossRef](#)]
35. Goodwin, N.R.; Collett, L.J. Development of an automated method for mapping fire history captured in Landsat TM and ETM+ time series across Queensland, Australia. *Remote Sens. Environ.* **2014**, *148*, 206–221. [[CrossRef](#)]
36. Hawbaker, T.J.; Vanderhoof, M.K.; Beal, Y.J.; Takacs, J.D.; Schmidt, G.L.; Falgout, J.T.; Williams, B.; Fairaux, N.M.; Caldwell, M.K.; Picotte, J.J.; et al. Mapping burned areas using dense time-series of Landsat data. *Remote Sens. Environ.* **2017**, *198*, 504–522. [[CrossRef](#)]
37. Long, T.; Zhang, Z.; He, G.; Jiao, W.; Tang, C.; Wu, B.; Zhang, X.; Wang, G.; Yin, R. 30 m Resolution Global Annual Burned Area Mapping Based on Landsat Images and Google Earth Engine. *Remote Sens.* **2019**, *11*, 489. [[CrossRef](#)]
38. Bar, S.; Parida, B.R.; Pandey, A.C. Landsat-8 and Sentinel-2 based Forest fire burn area mapping using machine learning algorithms on GEE cloud platform over Uttarakhand, Western Himalaya. *Remote Sens. Appl. Soc. Environ.* **2020**, *18*, 100324. [[CrossRef](#)]
39. Gorelick, N.; Hancher, M.; Dixon, M.; Ilyushchenko, S.; Thau, D.; Moore, R. Google Earth Engine: Planetary-scale geospatial analysis for everyone. *Remote Sens. Environ.* **2017**, *202*, 18–27. [[CrossRef](#)]
40. Arruda, V.L.S.; Piontekowski, V.J.; Alencar, A.; Pereira, R.S.; Matricardi, E.A.T. An alternative approach for mapping burn scars using Landsat imagery, Google Earth Engine, and Deep Learning in the Brazilian Savanna. *Remote Sens. Appl. Soc. Environ.* **2021**, *22*. [[CrossRef](#)]
41. Melchiori, A.E.; Cândido, P.A.; Libonati, R.; Morelli, F.; Setzer, A.W.; de Jesus, S.C.; Fonseca, L.M.G.; Körting, T.S. Spectral indices and multi-temporal change image detection algorithms for burned area extraction in the Brazilian Cerrado. In Proceedings of the Anais XVII Simpósio Brasileiro de Sensoriamento Remoto—SBSR, João Pessoa-PB, Brasil, 25–29 April 2015; pp. 643–650. [[CrossRef](#)]
42. Roteta, E.; Bastarrika, A.; Franquesa, M.; Chuvieco, E. Landsat and Sentinel-2 Based Burned Area Mapping Tools in Google Earth Engine. *Remote Sens.* **2021**, *13*, 816. [[CrossRef](#)]
43. Mazher, A.; Li, P.; Zhang, J. Mapping burned areas from Landsat TM images: A comparative study. In Proceedings of the International Conference on Computer Vision in Remote Sensing, Xiamen, China, 16–18 December 2012; pp. 285–290.
44. Moya, M.M.; Hush, D.R. Network constraints and multi-objective optimization for one-class classification. *Neural Netw.* **1996**, *9*, 463–474. [[CrossRef](#)]
45. Alonso-Canas, I.; Chuvieco, E. Global burned area mapping from ENVISAT-MERIS and MODIS active fire data. *Remote Sens. Environ.* **2015**, *163*, 140–152. [[CrossRef](#)]
46. Alvarado, S.T.; Fornazari, T.; Cóstola, A.; Morellato, L.P.C.; Silva, T.S.F. Drivers of fire occurrence in a mountainous Brazilian cerrado savanna: Tracking long-term fire regimes using remote sensing. *Ecol. Indic.* **2017**, *78*, 270–281. [[CrossRef](#)]
47. Alvarado, S.T.; Silva, T.S.F.; Archibald, S. Management impacts on fire occurrence: A comparison of fire regimes of African and South American tropical savannas in different protected areas. *J. Environ. Manag.* **2018**, *218*, 79–87. [[CrossRef](#)] [[PubMed](#)]
48. Carvalho, L.M.T.; Oliveira, M.S.; Alves, M.C.; Vianello, R.L. Flora. In *Zoneamento Ecológico-Econômico do Estado de Minas Gerais: Componentes Geofísico e Biótico*; UFLA: Lavras, Brasil, 2008; pp. 137–150. ISBN 9788587692535.
49. Pereira, A.A.; Rodrigues Teixeira, F.; Libonati, R.; Melchiori, E.A.; Carvalho, L.M.T. No 68/8: 1665-1680 Sociedade Brasileira de Cartografia, Geodésia, Fotogrametria e Sensoriamento Remoto Recebido em 16 de Outubro. *Rev. Bras. Cartogr.* **2016**, *68*, 8.
50. Silveira, F.A.O.; Negreiros, D.; Barbosa, N.P.U.; Buisson, E.; Carmo, F.F.; Carstensen, D.W.; Conceição, A.A.; Cornelissen, T.G.; Echternacht, L.; Fernandes, G.W.; et al. Ecology and evolution of plant diversity in the endangered campo rupestre: A neglected conservation priority. *Plant Soil* **2016**, *403*, 129–152. [[CrossRef](#)]
51. da SILVA, A.M.; MELLO, C.R. Nível de comprometimento da água. In *Zoneamento Ecológico-Econômico do Estado de Minas Gerais: Zoneamento e cenários exploratórios*; SCOLFORO, J.R.S., OLIVEIRA, A.D., CARVALHO, L.M.T., Eds.; EDITORA DA UFLA: Lavras, Brasil, 2008; Volume 1, pp. 37–52.

52. Valadão, R.C.; de Oliveira, C.V.; Ker, J.C. Compartimentação regional do relevo e cobertura pedológica do centro-norte de Minas Gerais. *Rev. Geogr.* **2008**, *93*–100. [[CrossRef](#)]
53. Carvalho, L.D.; Silva, M.; Alves, M.D.C.; Vianello, R.L.; Sediya, G.C.; Castro Neto, P.; Dantas, A.A.A. Clima. In *Zonamento Ecológico- Econômico do Estado de Minas Gerais: Componentes Geofísico e Biótico*; UFLA: Lavras, Brasil, 2008; pp. 89–102. ISBN 9788587692535.
54. United States Geological Survey Database. Available online: <https://earthexplorer.usgs.gov/> (accessed on 5 February 2021).
55. Schroeder, W.; Oliva, P.; Giglio, L.; Csiszar, I.A. The New VIIRS 375 m active fire detection data product: Algorithm description and initial assessment. *Remote Sens. Environ.* **2014**, *143*, 85–96. [[CrossRef](#)]
56. Brazilian Institute of Spatial Research (INPE) Active Fires Database. Available online: <http://queimadas.dgi.inpe.br/queimadas/bdqueimadas> (accessed on 5 February 2021).
57. Brazilian Institute of Spatial Research (INPE) Burned Area Database. Available online: <http://queimadas.dgi.inpe.br/queimadas/aq30m/> (accessed on 5 December 2020).
58. Schölkopf, B.; Smola, A.J.; Williamson, R.C.; Bartlett, P.L. New support vector algorithms. *Neural Comput.* **2000**, *12*, 1207–1245. [[CrossRef](#)]
59. Schölkopf, B.; Williamson, R.; Smola, A.; Shawe-Taylor, J.; Piatt, J. Support vector method for novelty detection. *Adv. Neural Inf. Process. Syst.* **2000**, 582–588.
60. Dragozi, E.; Gitas, I.Z.; Stavrakoudis, D.G.; Theocharis, J.B. Burned area mapping using support vector machines and the FuzCoC feature selection method on VHR IKONOS imagery. *Remote Sens.* **2014**, *6*, 12005–12036. [[CrossRef](#)]
61. Cabral, A.; de Vasconcelos, M.J.P.; Pereira, J.M.C.; Bartholomé, É.; Mayaux, P. Multi-temporal compositing approaches for SPOT-4 vegetation. *Int. J. Remote Sens.* **2003**, *24*, 3343–3350. [[CrossRef](#)]
62. Carreiras, J.M.B.; Pereira, J.M.C. SPOT-4 VEGETATION multi-temporal compositing for land cover change studies over tropical regions. *Int. J. Remote Sens.* **2005**, *26*, 1323–1346. [[CrossRef](#)]
63. McKeeman, W.M. Peephole optimization. *Commun. ACM* **1965**, *8*, 443–444. [[CrossRef](#)]
64. McMaster, R.; McMaster, S. A history of twentieth-century American academic cartography. *Cartogr. Geogr. Inf. Sci.* **2002**, *29*, 305–321. [[CrossRef](#)]
65. Pereira, A.A.; Carvalho, L.M.T.; Libonati, R.; Acerbi Júnior, F.W.; Morelli, F. Avaliação de nove índices espectrais quanto a separabilidade entre queimadas e diferentes alvos. In Proceedings of the XVIII Simpósio Brasileiro Sensoriamento Remoto—SBSR, João Pessoa-PB, Brasil, 25–29 April 2015; pp. 3105–3112.
66. Franquesa, M.; Vanderhoof, M.K.; Stavrakoudis, D.; Gitas, I.Z.; Roteta, E.; Padilla, M.; Chuvieco, E. Development of a standard database of reference sites for validating global burned area products. *Earth Syst. Sci. Data* **2020**, *12*, 3229–3246. [[CrossRef](#)]
67. Mayr, S.; Kuenzer, C.; Gessner, U.; Klein, I.; Rutzinger, M. Validation of earth observation time-series: A review for large-area and temporally dense land surface products. *Remote Sens.* **2019**, *11*, 2616. [[CrossRef](#)]
68. Stroppiana, D.; Bordogna, G.; Carrara, P.; Boschetti, M.; Boschetti, L.; Brivio, P.A. A method for extracting burned areas from Landsat TM/ETM+ images by soft aggregation of multiple Spectral Indices and a region growing algorithm. *ISPRS J. Photogramm. Remote Sens.* **2012**, *69*, 88–102. [[CrossRef](#)]
69. Lillesand, T.M.; Kiefer, R.W. *Remote Sensing and Image Interpretation*, 3rd ed.; John Wiley and Sons, Inc.: Hoboken, NJ, USA, 1994; p. 750.
70. Roy, D.P.H.; Frost, P.G.; Justice, C.O.; Landmann, T.; Le Roux, J.L.; Gumbo, K.; Makungwa, S.; Dunham, K.; Toit, R.D.U.; Mhwandagaraii, K.; et al. The Southern Africa Fire Network (SAFNet) regional burned-area product-validation protocol. *Int. J. Remote Sens.* **2005**, *26*, 4265–4292. [[CrossRef](#)]
71. Durigan, G. Zero-fire: Not possible nor desirable in the Cerrado of Brazil. *Flora Morphol. Distrib. Funct. Ecol. Plants* **2020**, *268*, 151612. [[CrossRef](#)]
72. Souza, C.M.; Shimbo, J.Z.; Rosa, M.R.; Parente, L.L.; Alencar, A.A.; Rudorff, B.F.T.; Hasenack, H.; Matsumoto, M.; Ferreira, L.G.; Souza-Filho, P.W.M.; et al. Reconstructing Three Decades of Land Use and Land Cover Changes in Brazilian Biomes with Landsat Archive and Earth Engine. *Remote Sens.* **2020**, *12*, 2735. [[CrossRef](#)]
73. Schmidt, I.B.; Moura, L.C.; Ferreira, M.C.; Eloy, L.; Sampaio, A.B.; Dias, P.A.; Berlinck, C.N. Fire management in the Brazilian savanna: First steps and the way forward. *J. Appl. Ecol.* **2018**, *55*, 2094–2101. [[CrossRef](#)]
74. Wulder, M.A.; White, J.C.; Goward, S.N.; Masek, J.G.; Irons, J.R.; Herold, M.; Cohen, W.B.; Loveland, T.R.; Woodcock, C.E. Landsat continuity: Issues and opportunities for land cover monitoring. *Remote Sens. Environ.* **2008**, *112*, 955–969. [[CrossRef](#)]
75. Campagnolo, M.L.; Libonati, R.; Rodrigues, J.A.; Pereira, J.M.C. A comprehensive characterization of MODIS daily burned area mapping accuracy across fire sizes in tropical savannas. *Remote Sens. Environ.* **2021**, *252*. [[CrossRef](#)]
76. Rodrigues, J.A.; Libonati, R.; Pereira, A.A.; Nogueira, J.M.P.; Santos, F.L.M.; Peres, L.F.; Santa Rosa, A.; Schroeder, W.; Pereira, J.M.C.; Giglio, L.; et al. How well do global burned area products represent fire patterns in the Brazilian Savannas biome? An accuracy assessment of the MCD64 collections. *Int. J. Appl. Earth Obs. Geoinf.* **2019**, *78*, 318–331. [[CrossRef](#)]
77. Ramo, R.; Roteta, E.; Bistinas, I.; van Wees, D.; Bastarrika, A.; Chuvieco, E.; van der Werf, G.R. African burned area and fire carbon emissions are strongly impacted by small fires undetected by coarse resolution satellite data. *Proc. Natl. Acad. Sci. USA* **2021**, *118*, e2011160118. [[CrossRef](#)]
78. Giglio, L.; Loboda, T.; Roy, D.P.; Quayle, B.; Justice, C.O. An active-fire based burned area mapping algorithm for the MODIS sensor. *Remote Sens. Environ.* **2009**, *113*, 408–420. [[CrossRef](#)]

-
79. Pereira, A.A.; Pereira, J.A.A.; Morelli, F.; Barros, D.A.; Acerbi, F.W.; Scolforo, J.R.S. Validation of hotspots utilized in the orbital monitoring of burnt areas by means of TM images. *Cerne* **2012**, *18*, 335–343. [[CrossRef](#)]
 80. Sano, E.E.; Rodrigues, A.A.; Martins, E.S.; Bettiol, G.M.; Bustamante, M.M.C.; Bezerra, A.S.; Couto, A.F.; Vasconcelos, V.; Schüler, J.; Bolfe, E.L. Cerrado ecoregions: A spatial framework to assess and prioritize Brazilian savanna environmental diversity for conservation. *J. Environ. Manag.* **2019**, *232*, 818–828. [[CrossRef](#)]